UNIVERSITY OF CALIFORNIA,
IRVINE

Enhancement of Spin Hall oscillator (SHO) power via giant magneto-resistance (GMR) effect

THESIS

submitted in partial satisfaction of the requirements
for the degree of

MASTER OF SCIENCE

in Chemical and Material Physics

by

Jen-Ru Chen

Thesis Committee:
Professor Ilya N. Krivorotov, Chair
Professor Wilson Ho
Professor Zuzanna S. Siwy

2018

TABLE OF CONTENTS

LIST OF FIGURES

ACKNOWLEDGMENTS

I would like to thank my advisor, Professor Ilya Krivorotov, who has been patient and supportive to guide me into the research. He is one of most knowledgeable physicists I have ever met. It has been a great pleasure to discuss with him and learn from him.

I also want to thank everyone in Ilya's group: Igor Barsukov, Eric Montoya, Zheng Duan, Brian Youngblood, Liu Yang, Yu-Jin Chen, Han Kyu Lee, Andrew Smith, Jieyi Zhang, Alejandro Jara, Chris Safranski, Josh Dill, and Chengcen Sha. I really enjoy the heritage of our group, which people respect to each other and help each other as much as they can in research.

CURRICULUM VITAE

Jen-Ru Chen

EDUCATION

Master of Science in Chemical and Material Physics **2018**
University of California, Irvine *Irvine, CA*

Master of Science in Physics **2007**
National Taiwan University *Taipei, Taiwan*

Bachelor of Science in Physics **2004**
National Taiwan University *Taipei, Taiwan*

RESEARCH EXPERIENCE

Graduate Research Assistant **2010–2013**
University of California, Riverside *Riverside, California*

Graduate Research Assistant **2013–present**
University of California, Irvine *Irvine, California*

TEACHING EXPERIENCE

Teaching Assistant **2010–2012**
University of California, Riverside *Riverside, California*

Teaching Assistant **2013–2014**
University of California, Irvine *Irvine, California*

REFEREED JOURNAL PUBLICATIONS

Jen-Ru Chen, Patrick M Odenthal, Adrian G Swartz, George Charles Floyd, Hua Wen, Kelly Yunqiu Luo, Roland K Kawakami., Control of Schottky barriers in single layer MoS_2 transistors with ferromagnetic contacts, *Nano letters* 13 (7), 3106 (2013)

REFEREED CONFERENCE PUBLICATIONS

Jen-Ru Chen, E. Montoya, H. K. Lee, C. Sha, R. Ngelale, H. W. Tseng, L. Wan, E. Yang, M. Nilsson, O. Boyraz, N. Bagherzadeh, and Ilya Krivorotov., Effect of Ionizing Radiation on CoFeB/MgO/CoFeB Nanoscale Magnetic Tunnel Junctions, *Magnetism and Magnetic Materials*, Oral (2017)

Jen-Ru Chen, Andrew Smith, and Ila Krivorotov., Enhancement of spin Hall oscillator (SHO) power via giant magneto-resistance (GMR) effect, *Magnetism and Magnetic Materials*, Oral (2016)

Jen-Ru Chen, P. Odenthal, and R. Kawakami., Electrical transport and contact characteristics of single layer MoS_2 devices, *APS meeting*, Oral (2013)

ABSTRACT OF THE THESIS

Enhancement of Spin Hall oscillator (SHO) power via giant magneto-resistance (GMR) effect

By

Jen-Ru Chen

Master of Science in Chemical and Material Physics

University of California, Irvine, 2018

Professor Ilya N. Krivorotov, Chair

Spin Hall effect in a heavy metal (HM) generates a pure spin current flowing perpendicular to an applied electric charge current. When injected into a ferromagnet (FM), this pure spin current can act as negative magnetic damping thereby exciting self-oscillations of magnetization. In a simple HM/FM bilayer geometry, the current-driven self-oscillations of magnetization result in a microwave voltage generation due to anisotropic magneto-resistance (AMR) of the FM. Since AMR in thin films of typical FM materials such as Permalloy (Py) is relatively small, the output microwave signal generated by the HM/FM bilayer spin Hall oscillators (SHOs) is typically limited to $\sim$ 0.1 nW. Here we report a new type of SHO by replacing FM layer with spin valve multilayers. In this type of devices, the microwave power generation relies on current-in-plane (CIP) giant magneto-resistance (GMR) instead of AMR. Since the magnitude GMR typically exceeds that of AMR, this new type of SHO can generate significantly higher power than the AMR-based SHOs. The maximum microwave power generated by the device exceeds 1 nW, which is over an order of magnitude higher than that in HM/FM bilayer SHO nanowire devices.

Chapter 1

Introduction

One of the most famous quotes of Issac Newton says, If I have seen further it is by standing on the shoulders of Giants. In 2007, Nobel Prize in Physics was awarded to Albert Fert and Peter Grunberg for the discovery of giant magnetoresistance (GMR) effect. This discovery has been opened tremendous studies on nanomagnetism and spintronics. The GMR-based multilayer structure also has been applied to make the read-head of hard drive and magnetic field sensors. In this dissertation, we studied the magnetic dynamics of nano-fabricated devices based on GMR effect, in which I appreciate we can stand on the shoulders of these respected Giants.

We investigate the dynamics of magnetization of GMR-based spin Hall oscillator (SHO) nanowire devices. The device structure combine with a heavy metal (HM) layer to the metallic spin valve multilayers, which consists of a free ferromagnet (FM), a normal metal (NM), and a pinned FM layers. The operation of these devices relies on the spin Hall effect (SHE), which converts the charge current flow in the plane of the HM layer into the pure spin current flow across the HM/FM interface. This pure spin current works as the anti-damping torque on the magnetization of the free FM layer and results in self-oscillations.

The microwave power generation is corresponded to current-in-plane (CIP) GMR, and the high output power is achieved. Moreover, the investigation of angular dependence of the GMR-based SHOs supports the enhancement of microwave output powers. In chapter 2, the basic background will be introduced to understand the behaviors and properties of the GMR-based SHOs. Chapter 3 shows the nano-fabrication of the nanowire devices, including the introduction of instruments and fabrication procedures. The motivation and the experimental results will be discussed in detail in chapter 4. Finally, conclude the study in chapter 5.

Chapter 2

Background

2.1 Giant Magnetoresistance (GMR)

In spintronics, Magnetoresistance (MR) is a very frequently mentioned word. Simply speaking, MR is the change in electrical resistance due to the change of magnetization amplitude and orientation. There are many different types of MR, and one of the most important ones is GMR. The discovery of GMR is initially in antiferromagnetic coupled Fe/Cr systems which Grunberg and Fert studied and won for the Nobel Prize in 2007.[2, 3] Now, of course, it is known that the antiferromagnetic coupling is not completely necessary for the GMR effect. More generally, GMR is the dependence of electrical resistance on the angles between the magnetization orientations of two ferromagnetic layers which are separated by a normal metal (NM) layer. The resistance is low for parallel (P) alignment, and high for anti-parallel (AP) alignment in collinear magnetization geometry. This concept has triggered the studies on a simply trilayer structure, or named metallic spin valve structure, and has been applied widely in magnetic memories and sensors. The GMR effect can be explained by spin-dependent electron scattering mechanism. Ideally, we can assume that at the interface

the scattering rate depends on the electrons spin orientation with respect to the local magnetizations. So in the top graphs of Fig. 2.1, it is assumed that only electrons with opposite spin orientation related to FM layer are scattered. This yields an increase of total number of scattering events, so increases the electrical resistance. ($R_2 > R_1$) The Mott two-current model for the electrical conductivity in metals can be introduced here to understand the GMR effect. [4] The bottom graphs of Fig. 2.1 shows the two-current channel model of trilayer structure correspond to the top graph. If the Mean free path for both spin directions is much larger than the layer thickness. We can represent the resistances of same-spin and opposite-spin channel as R_1 and R_2. So the resistances for the P and AP cases are $R_p = 2R_1R_2/(R_1 + R_2)$ and $R_{ap} = (R_1 + R_2)/2$. The GMR ratio can be expressed as

$$\begin{aligned} GMR &= \frac{R_{ap} - R_p}{R_p} \\ &= \frac{(R_1 - R_2)^2}{4R_1R_2} \end{aligned} \tag{2.1}$$

For most of the general systems, $R_1, R_2 > 0$. It follows that $R_{ap} > R_p$, so the GMR ratio is positive.

2.2 Spin Hall Effect

It was proposed that when an electrical current circulates in a paramagnetic metal should lead to a transverse spin current in the system, called Spin Hall Effect (SHE). [5–7] The SHE originates from the spin-orbit interaction in metals and semiconductors. When an electron flow through a non-magnetic metal and encounter a local potential due to the large spin-orbit coupling of existing impurities or defects, the local potential causes a spin-asymmetry scattering of the electron. The electron will acquire a transverse velocity depends on the spin orientation. Fig. 2.2 shows the schematic graph of the SHE. In this simple explanation, the

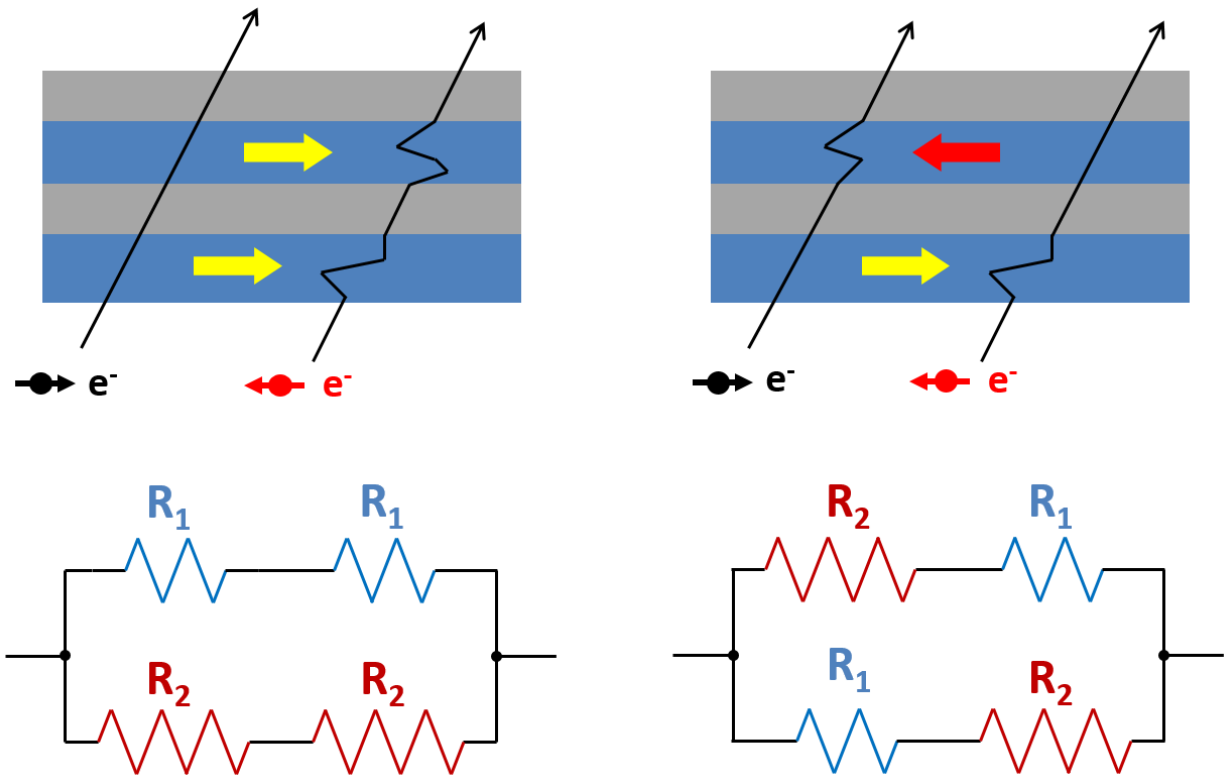

Figure 2.1: **Top:** The schematic drawings of two spin polarity electrons going through FM/NM/FM multilayers. The left graph shows parallel (P) state of two FM layers. The electron with the same spin orientation as the FM layers pass through this multilayer straightly while the electron with opposite spin orientation is largely scattered when passing through FM layer. The right graph shows anti-parallel (AP) state. Both electrons go straight through in one layer and scatter in another layer. **Bottom:** The Mott two-current model of P and AP states of FM/NM/FM structure correspond to the tops. The same-spin and opposite-spin channel is represented as R_1 and R_2.

red arrows are spin up electrons and the green ones represent spin down electrons, and the spin imbalance leads to the spin accumulation in both edges, i.e. $y = 0$ and $y = L$. SHE can be separated to intrinsic SHE and extrinsic SHE according to its mechanisms. The difference between the intrinsic and extrinsic SHE is similar to the mechanisms of spin relaxation. For intrinsic SHE, the electrons are affected by local potentials and acquire a transverse velocity in between the scattering events. While a transverse velocity or displacement is generated by electrons during the scattering event are referred to as extrinsic SHE. The impurity concentration is essential for SHE in normal metal systems. Due to the different dependence of Spin Hall conductivity to the different mechanisms of SHE, both intrinsic and extrinsic

SHE can contribute to the SHE in different metal systems. As a consequence, charge current in a normal metal system can be converted to pure spin current, which could be applied in all kinds of spintronic systems. The efficiency of converting charge current to spin current depends on the quality and the elements of metals. In general, heavy metals (HMs) have an averaged higher Spin Hall angle due to stronger spin-orbit coupling. So here we use the HM, platinum (Pt), which has a good conductivity and high spin Hall angle, to combine with FM multilayer for the study of spin Hall oscillator system.[7]

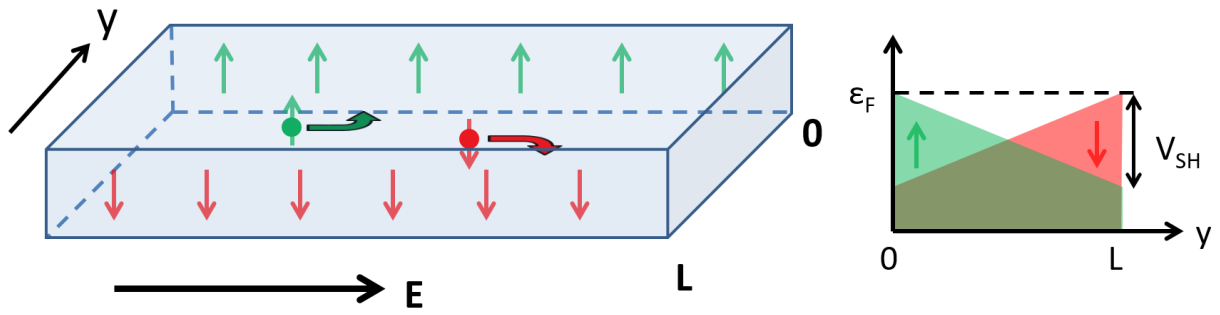

Figure 2.2: The schematic of spin Hall effect (SHE). The spin-up (green) and spin-down (red) charge carriers are deflected perpendicular from its original trajectories and imbalance accumulated to the two edges $y = 0$ and $y = L$. The right graph shows that the electric voltages at two edges are the same, V_{SH}, however spin dependent chemical potential differently.

2.3 Spin Transfer Torque (STT) and Magnetization Dynamics

In 1996, the effect of spin transfer torque (STT) in a magnetic multilayer system had been predicted by Slonczewski [8], which suggests that the flow of spin polarized electric current can excite the magnetic states of ferromagnets (FMs) due to exchange interactions. We can use a simple schematic example to understand STT, shown in Fig. 2.3.

When a conduction current is applied through a magnetic multilayer, it is polarized by first

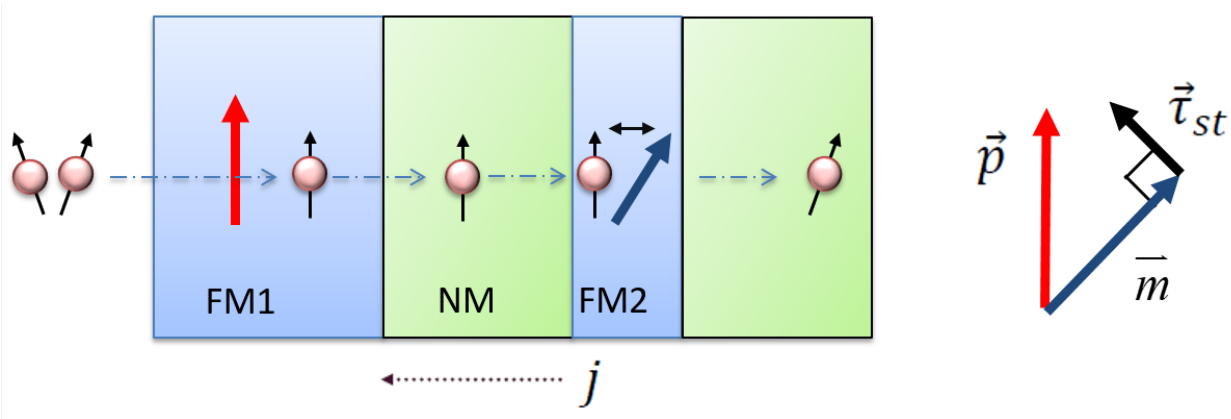

Figure 2.3: A example schematic shows spin transfer torques (STTs). The random spin electron current is polarized when pass through the FM1. This spin polarized current is transferred to FM2 and exert torque to local magnetic moment due to exchange interaction. After interaction, both magnetization in FM2 and transferred carriers change its spin orientations.

FM layer (FM1) and transported to the second FM layer (FM2). If the spin polarized current is differ from the direction of local magnetic moments in the FM2 layer, they exert torques onto each other and cause deflections from their original directions. This torque is called spin transfer torque, $\tau_s t$, denotes by black arrow in the right graph. The local magnetic moment in FM2 is express by the blue arrow, $\vec{m}$. The polarization of electron current is denotes by red arrow, $\vec{p}$. For conduction current, it carries the spin information of the local moments and interact with other magnetic moments after passing the FM2 layer. For the local magnetic moment in the FM2, it could have three possible results. First, if the STT torque is too small and not continuously applied on the local moment, the magnetization will differ from its original direction and relax back to its local minimum. Second, if the STT happens to be the cancellation of the magnetic damping torque of the magnetization, the local moments could stay deviated from its local minimum and start the precession motion. Finally, if the STT is overwhelming the damping of the system, it could cause the switching of the local moments to another local minimum. These results are schematically shown in Fig. 2.4. [1]

Here, I describe this STT behaviors with some assumptions and intrinsic properties of the

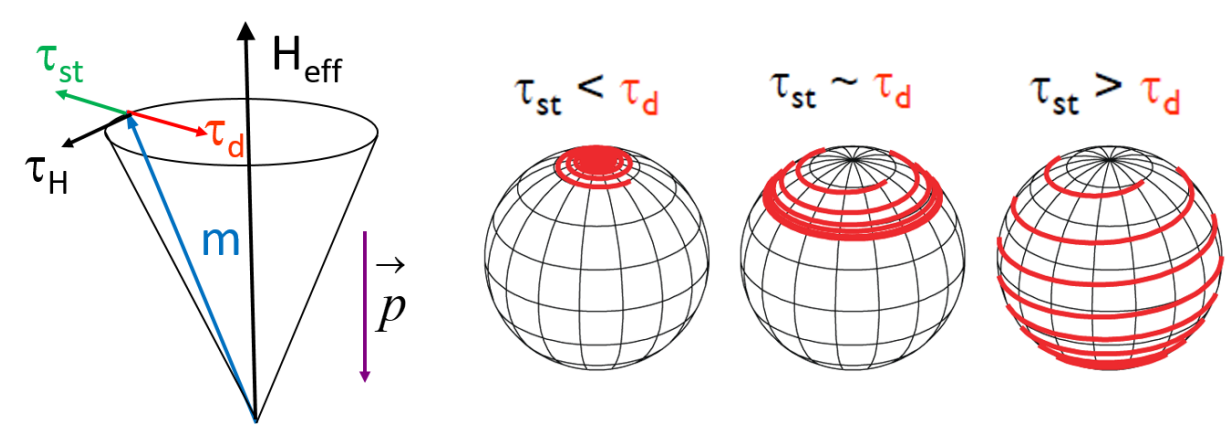

Figure 2.4: Illustration of the affection of spin transfer torque (STT) that leads to different motions of magnetic moment. If $\tau_{st} < \tau_d$, the magnetic moment relax back to its equilibrium. If $\tau_{st} \approx \tau_d$, the magnetic moment moves along a stable trajectory and self-oscillates. If $\tau_{st} > \tau_d$, the magnetic moment could oscillates in a larger and larger trajectory and eventually switches to another equilibrium position. [1]

system. For example, a system can have just one or two local minimums, it depends on geometry, material property, composition, and an external applied field of a system. So let's introduced the Landau-Lifshitz-Gilbert (LLG) equation [9, 10] to describe the equation of motion of single magnetic moment (with magnetization m) in a multilayer metallic spin valve system.

$$\begin{aligned} \frac{d\vec{m}}{dt} &= -\gamma\vec{m} \times \vec{H}_{eff} + \frac{\alpha}{|\vec{m}|}\vec{m} \times \frac{d\vec{m}}{dt} + \eta\frac{\mu_B I}{eV}\vec{m} \times (\vec{p} \times \vec{m}) \\ &= \tau_H + \tau_d + \tau_{st} \end{aligned} \tag{2.2}$$

The first term of this equation is field like torque which usually is small and can be ignored mostly in this metallic spin valve system. The second term is damping like torque, in which α is the Gilbert damping parameter. [10] This torque tends to pull the magnetization toward its equilibrium position. The third term is the STT. As we mentioned in this section STT can excite dynamics of magnetization once STT is comparable to damping like torque of a system. The continuous precession motion of a magnetic moment is usually a GHz auto-

oscillations which will be further discussed in next section.

2.4 Spin Torque Oscillator (STO) and Spin Hall Oscillator (SHO)

Spin torque oscillator (STO) is a special nanoscale magnetic device in which its magnetization is excited and auto-oscillated when the damping torques are compensated by the spin transfer torques (STTs). The conventional STOs are widely understood in current perpendicular-to-plane (CPP) metallic spin valves and magnetic tunnel junctions (MTJs). The oscillation of magnetization in these system is basically the change of MR (GMR or TMR), thus the auto-oscillation can be detected electrically as a microwave voltage. Another new type of STOs, called Spin Hall oscillator (SHO), is also introduced here. Since we know that the excitation of oscillation is induced by spin carriers which exchange interact with the local moment, it doesn't matter that the spin current comes from a polarized current or other ways. We have learned that spin Hall effect (SHE) in a heavy metal (HM) layer can create pure spin current transverse to bias current direction. So SHOs which rely on SHE induced spin current to excite self oscillations are studied by combining the HM layer to FM layer or magnetic multilayer.

Chapter 3

Nano-devices Fabrication

Most of the experiments in this thesis were carried out on fabricated nanowire devices of multilayer thin films. The sample structure is Sapphire(substrate)/IrMn(4 nm)/Co(2 nm)/Cu(4 nm)/Co(0.5 nm)/Py(3.5 nm)/Pt(5 nm). Here, the details of fabrication procedures and instruments are introduced.

3.1 Sputtering Deposition

Sputtering deposition uses argon plasma to eject small amount of source material then deposit onto a surface (substrate) while placing substrate in the trajectory of ejected material. Conductive material can be deposited by using DC power supply and insulator material can be deposited by using RF power source. The reason why the RF (13.56 MHz) power source is used is to accelerate argon plasma and get rid of the accumulated charges on the insulating target surface. The sputtering deposition is usually performed in an ultra high vacuum(UHV) chamber. By using the magnetic field to confine charged particles (Ar plasma), it enhances both the efficiency of the initial ionization process and also allows plasma to be generated

at lower pressures which can reduce the deposition rate of materials. This is named as magnetron sputtering. The Base pressure of the sputtering deposition system in our lab can reach 5×10^{-9} torr. The few-nanometer thin films with uniformity close to the substrate can be deposited by flowing low pressure argon gas into the chamber and modifying power levels. For our system, the deposition rate is quite stable for a given power. The precise values can be extracted out by measuring the thickness of thin films. Figure 3.1 is the schematic and a picture of sputtering deposition system.

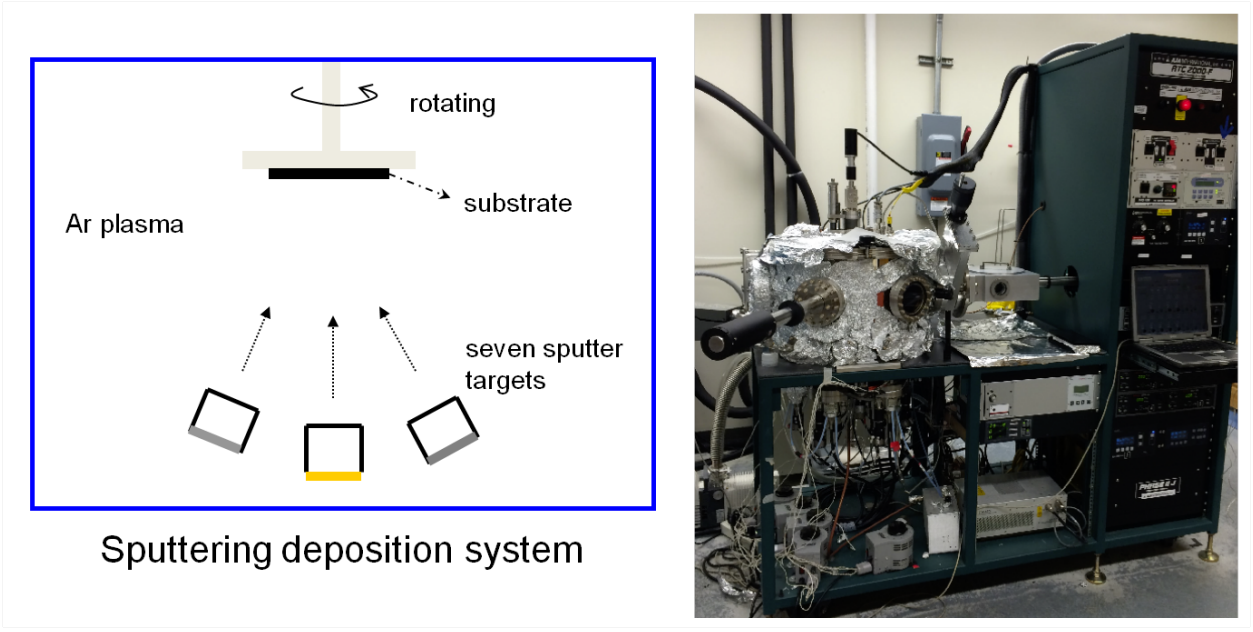

Figure 3.1: **Left:** The mechanism of sputtering deposition system. **Right:** The pictures of AJA magnetron sputtering system in the Lab.

3.2 Electron Beam Evaporation

Here, we introduce another way to deposit multilayer thin films, electron beam evaporation (E-beam evaporation). Unlike sputtering deposition that we use for growing couples of nanometer materials. The E-beam evaporation can be used for depositing tens of nanometer to microns of materials. E-beam evaporation is a form of physical vapor deposition. Basically, an intense electron beam is generated from a high voltage charged filament and accelerated via electric and magnetic field to a target material. The kinetic energy of electrons is transferred to the target material, which vaporized the material in a high vacuum chamber. This vapor can be used to coat a substrate positioned above the evaporating material. The E-beam evaporation was used to deposit alignment marks and contact leads on the device structures. The material combinations can be Ti/Au, Cr/Au, or Al/Au. The first layer (Ti, Cr, Al) is the adhesion layer with the thickness from 5 to 10 nm. The gold layer, with the thickness from 30 to 60 nm usually, offers a good contact for electrical conducted measurement.

3.3 Scanning Electron Microscopy and Electron Beam Lithography

A scanning electron microscopy(SEM) uses focused electron beam to scan sample's surfaces to create an image. The electrons interact with solid samples and generate signals which include information of sample's surface topography and chemical compositions. The most command signal that reveal sample's surface image is secondary electrons. The high energy electron beam interacts with the atoms of sample surface and excite the energy states of atoms. Then, the lower energy electrons are emitted by these atoms when the atoms fall back to their ground states. These emitted electrons are called secondary electrons which

are detected and compose a 2-dimensional image. Figure 3.2 is an example of SEM image of a Sb_2Te_3 nanoribbon. One of the most important applications of SEM is electron beam lithography (EBL), which uses focused electron beam to write a pattern on a thin-layer of E-beam resist. Depends on the types of resists, the pattern or mask can be developed. This resist-composed pattern or mask structure could be used for deposit materials onto it. Then, after a lift-off procedure to remove the resist, a pattern of desired materials shows up on the substrate. This technique can create nanoscale devices for different desired measurements and applications.

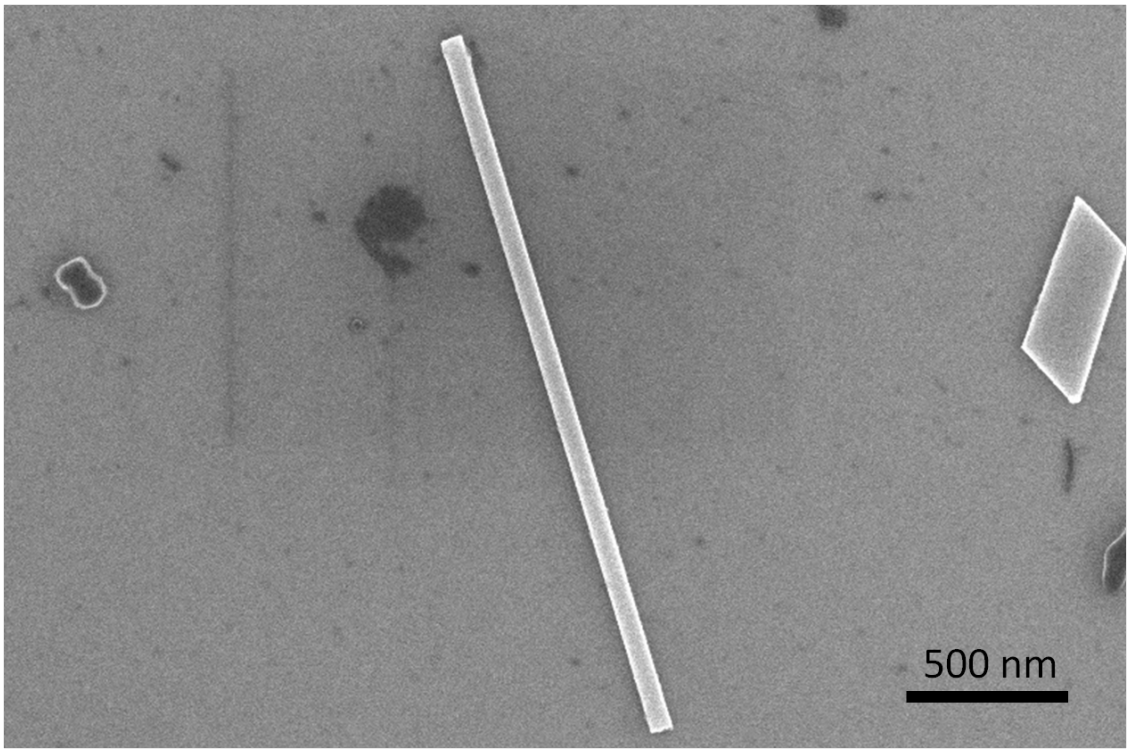

Figure 3.2: The SEM image of a Sb_2Te_3 nanoribbon. The scale bar is 500 nm.

3.4 Ion Milling

In general, etching process is an essential procedure for micro- or nano-fabricated devices. Usually it can be categorized to two groups, wet etch or dry etch. Depends on the materials

and structures, we can choose the most efficient and reliable methods to perform etching process. The dry ion beam milling used to be the good way for etching of nano-sized structure due to the repeatability and precision. In general, the ion milling can simply pictured as an atomic sand blaster by using accelerated Argon ions to bombard target surface. Due to the rotation of sample stage and the changeable stage angles, ion milling etching process can create clean and straight side walls of samples. This method is beneficial to determine the nanowire geometry in our study.

3.5 In-Filed Oven Annealing

Set-up the reference ferromagnetic layer orientation is needed of the GMR spin-valve structure devices. Usually, there are two ways to determine the reference layer orientation of the spin-valve structure we focused above. We can do the deposition with a magnetic field applied during the process or do the post annealing in a magnetic field. Here, we perform the post annealing in a special sample holder with strong permanent magnets to apply the magnetic field. The annealing procedure is in a high power oven equipped with a pumping station. The oven chamber is capable to anneal at ambient temperature 300°C in 2.4×10^{-6} torr high vacuum environment.

3.6 Device Fabrication Procedures

The schematic of nano-fabrication procedures of a multilayer nanowire device is shown in Fig. 3.3.

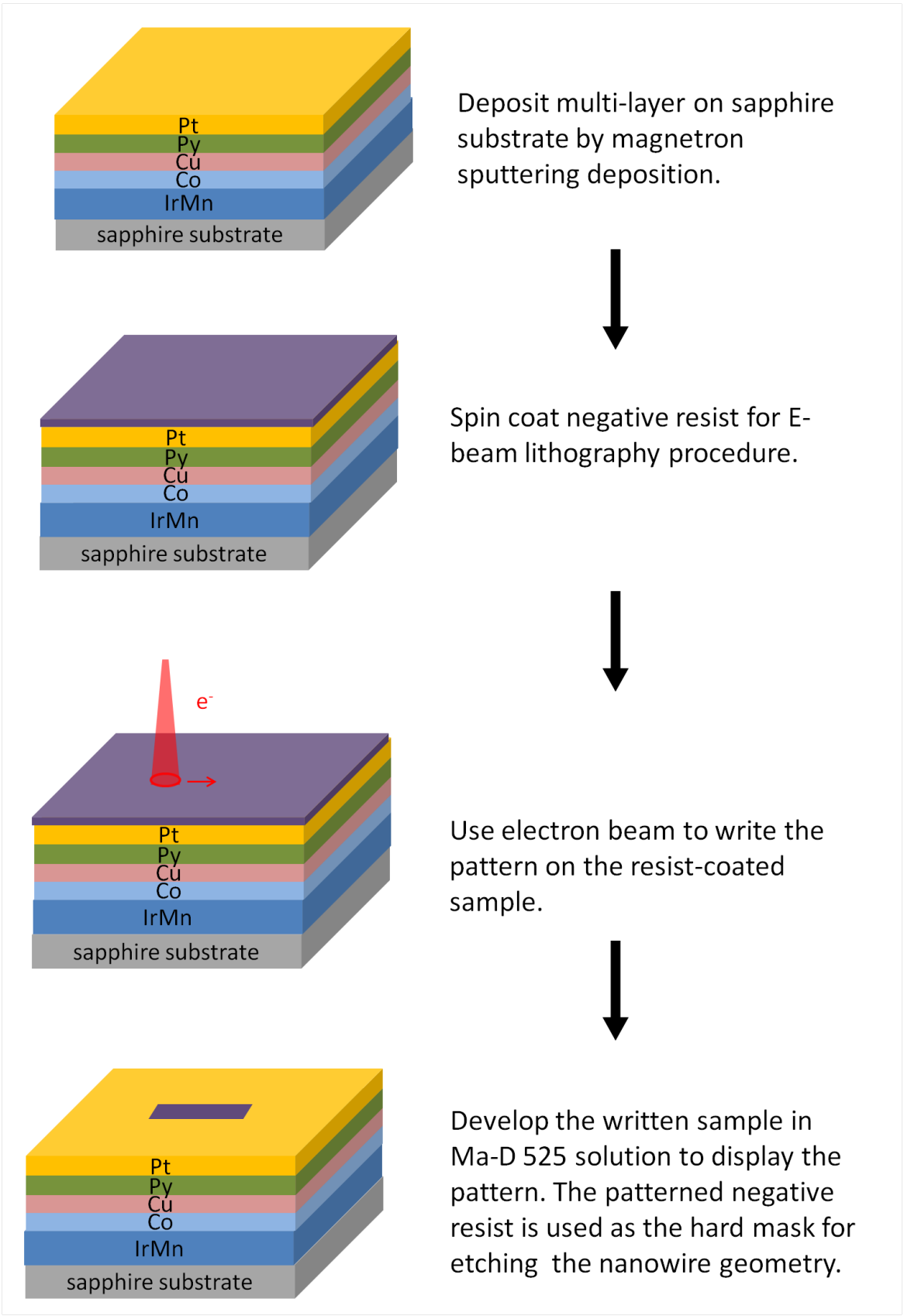

Figure 3.3: Nano-fabrication procedures.

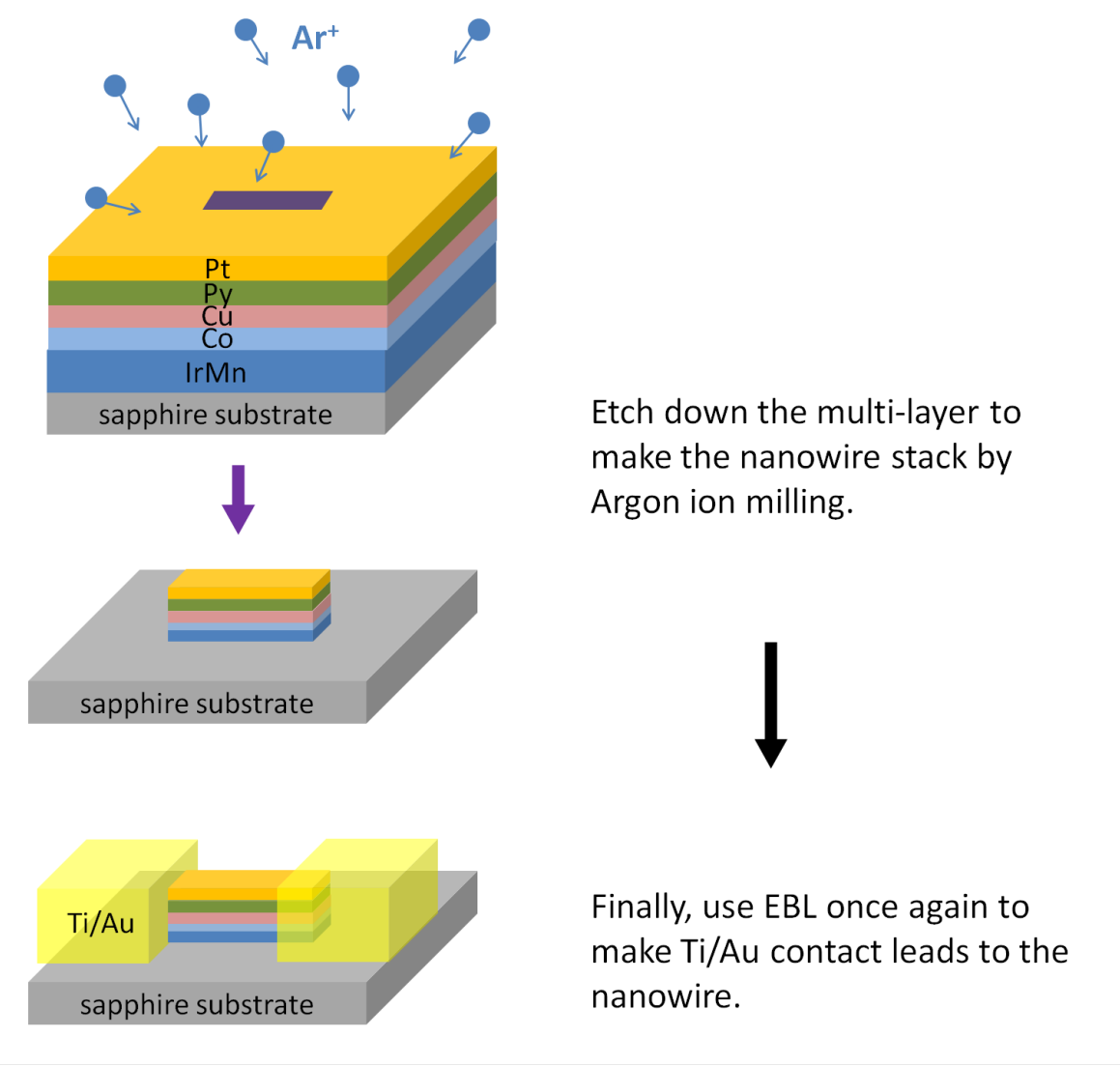

Figure 3.4: Nano-fabrication procedures.

Chapter 4

GMR-based and AMR-based SHOs

4.1 Introduction

STOs which rely on spin angular momentum exerts on a FM to excite magnetization self oscillations have great potential for applications in communication, navigation, and microwave sensing systems.[8, 11–17] Recent observations of a new type of STOs have attracted a lot of interests due to its simple and flexible design of devices. Based on spin Hall effect (SHE) [5–7, 18–21], a lateral current in a non-magnetic layer generates transverse pure spin current, the adjacent FM layer is excited by spin orbit torques and self-oscillates to generate microwave AC signals. Recent studies on Pt-metallic FM devices with different geometries [22–28] and Pt-magnetic insulator system [29] also indicate that that these current-in-plane (CIP) SHOs have comparable characteristics and advantages to STOs.

One of the key reasons that obstacle SHOs toward the real application is the magnitude of microwave output powers. From the studies up to date of STOs, the system which based on magnetic tunnel junctions (MTJs) demonstrates higher output powers up to 0.1 to 10 μW. [30–34] However, due to the nature of quantum behavior of MTJs, tunneling

magneto-resistance (TMR) effect arisen from highly polarized, non-scattered tunneling current requires current perpendicular to the plane (CPP) geometry of the device. This limited the possibility by applying lateral SHE into MTJs-based system, thus the nanoscale MTJ device fabrication becomes a consumable and complicate process. Let alone there is an issue related to impedance mismatch to RF circuits of TMR-based STO systems. Since conventional CPP-GMR STO devices usually provides reasonable microwave power output with narrower linewidth oscillation modes [35–39], we suggest to apply CIP-GMR structure into SHO system. To our knowledge, this GMR-based SHO system could be the biggest power boost among the lateral SHO systems.

In this dissertation, we investigate the dynamics of magnetization of GMR-based SHO nanowire devices. The device structure combine with Pt layer to the metallic spin valve multilayers, which consists of a free FM, a normal metal (NM), a pinned FM, and an antiferromagnetic (AFM) layers. Figure 4-1(b) shows the schematics of this SHO system. The comparison to the bi-layer (HM/FM) SHO device is also included.(The schematic shows in Fig. 4-1(a)) The operation of these devices relies on the SHE, which converts the charge current flow in the plane of HM layer into the pure spin current flow across the HM/FM interface. This pure spin current works as the anti-damping torque on the magnetization of free FM layer and results in self-oscillations. The self-oscillation corresponds to the resistance oscillation of MR. Fig. 4-1(c) and (d) show the angular dependence of AMR and GMR. If the equilibrium direction of magnetization is fixed at 90 degree, the spin Hall effect induced spin current direction, the oscillations happens at the red circle point for both GMR and AMR SHOs. The AC resistance difference (δR_{ac}) is obviously larger at the incline slop position for GMR angular curve than the valley position for AMR angular curve. Therefore, the investigation of angular dependence of the GMR-based SHOs supports the enhancement of output powers. It also reveals the most efficient consuming of spin orbit torque while in operation of these devices. Moreover, the microwave power generation is corresponded to CIP GMR. Since the GMR value is usually larger than the AMR, the microwave power

output of GMR SHO is far above the power output by any bilayer AMR-based SHO systems. The maxima power output achieved of GMR SHOs is 2 nW in our studies.

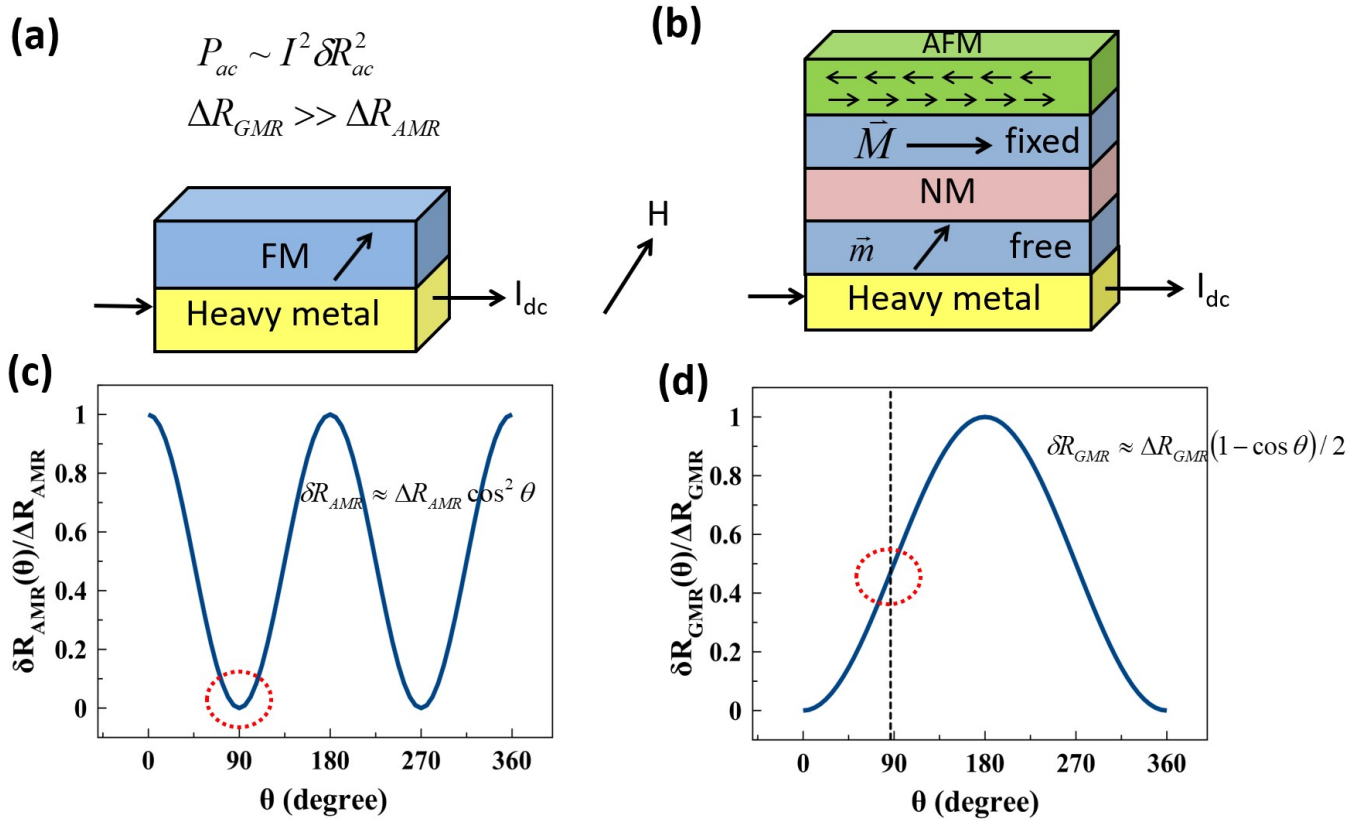

Figure 4.1: **(a)** The schematic of AMR-based SHO structure which includes one FM layer and one HM layer. The in-plane DC current flow through the HM layer to generate spin current in in-plane perpendicular direction via Spin Hall effect and add onto the FM layer. The top two equation simply imply the behavior that AC output power is proportional to resistance oscillation. The amplitude of resistance oscillation comes from MR, which is GMR or AMR here. And the GMR magnitude is much larger than AMR magnitude. **(b)** The schematic of GMR-based SHO structure, which includes a free FM layer, a normal metal (NM) layer, a fixed FM layer and a AFM layer. **(c)** The normalized AMR angular dependence plot. The AMR variance is proportional to $cos(\theta)^2$. **(d)** The normalized GMR angular dependence plot. The GMR variance is proportional to $(1 - cos(\theta))/2$.

4.2 SHO nanowire devices, GMR and Spectrum

The GMR-based SHO nanowire devices were patterned from a sapphire (substrate)/IrMn (4)/Co (2)/Cu (4)/Co (0.5)/Py (3.5)/Pt (5) multilayer (thickness in nanometers), which was deposited by magnetron sputtering. The 0.5 nm cobalt layer was inserted in between Cu and Py layer to modify the interface and enhance the GMR ratio. [40] This metallic spin valve multilayer was processed with an in-field post annealing at 250°C for 1 hour to determine the orientation of pinned FM layer (Co layer) by AFM exchange bias pinning effect [41, 42]. The magnetization orientation of Co layer was along the nanowire axis and defined as the easy axis. The geometry of nanowire was defined by using e-beam lithography and Argon ion milling. The width was 65 nm and the length was 40 μm in order to approximate the demagnetization field close to zero along the wire axis. The device was fabricated to have a 740 nm microwave emission active region in between the two attached Ti (5 nm)/Au (40 nm) contact leads. Fig. 4.2(a) shows the scanning electron microscopy (SEM) image and the layer structure of the GMR-based SHO device. The AMR-based SHO nanowire device was also fabricated with a similar geometry (width 70 nm, active region 650 nm) shown in Fig. 4.2(b). This control sample was made from the sapphire (substrate)/Cu (4)/Co (0.5)/Py (3.5)/Pt (5) multi-layers. By adding the Cu layer in this control sample, we can keep similar current density flow through the Pt layer to excite self-oscillations.

For the GMR-based SHO nanowire and the AMR-based SHO nanowire, the electrical measurements were performed in a cryogenic system at liquid helium temperature (4.2 K). The magneto-resistance (MR) curves were investigated of both devices by sweeping an external magnetic field along the easy (hard) axis. The MR difference of GMR-based SHO nanowire is about 10 times larger than the value of AMR-base SHO nanowire. The GMR effect with the field along the easy and hard axis of the device are shown in Fig. 4.3(a) and Fig. 4.3(b). Fig. 4.4 shows the AMR value with the field applied perpendicular to the nanowire axis. Since the microwave signal, $V_{ac} \approx I_{dc}\delta R_{ac}$, is generated from the self-oscillations of magnetization

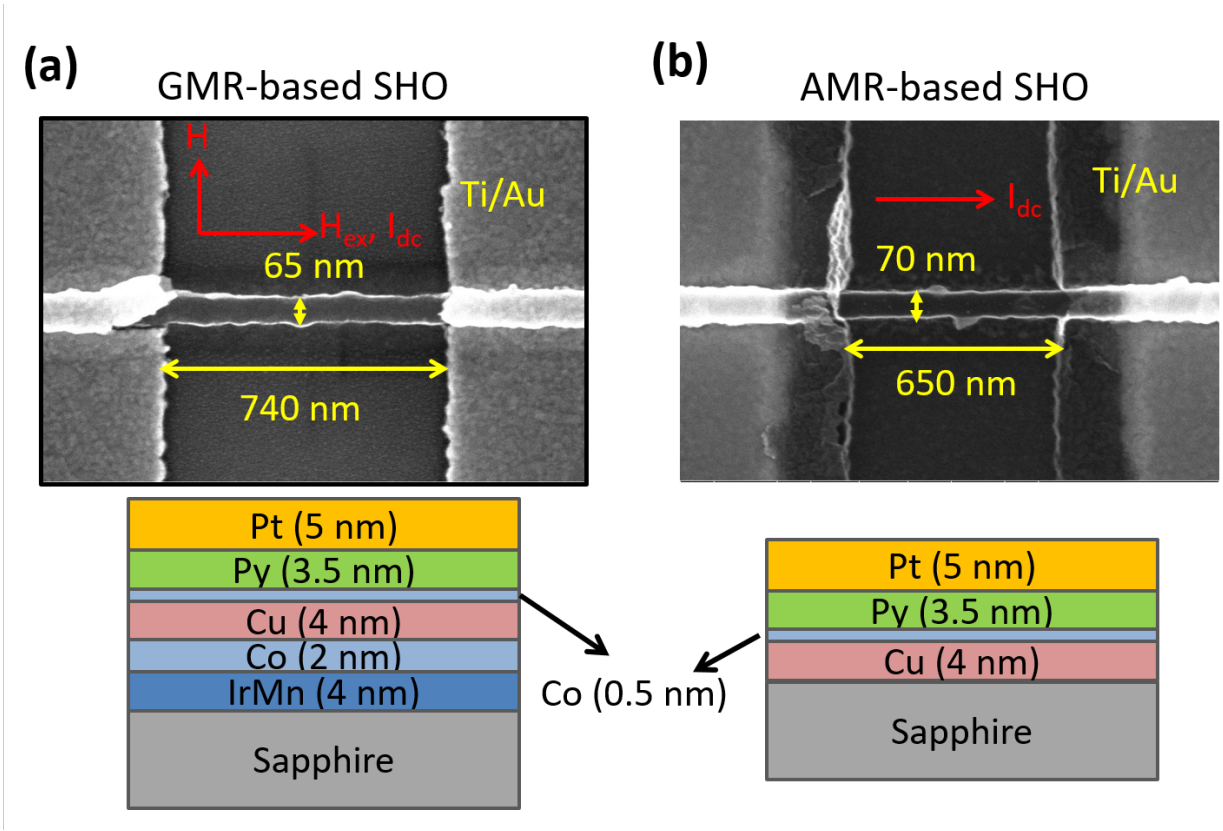

Figure 4.2: **(a)/(b)** The scanning electron microscopy (SEM) image of GMR/AMR-based SHO nanowire device and it's multilayer structure showing on the bottom.

that is magneto-resistance oscillations (δR_{ac}). Therefore, the microwave emission power of GMR-based SHO is expected to be much larger than that of AMR-based SHO based on the MR values.

Fig. 4.5 shows the microwave emission spectrum of the devices. A dc current was applied to the device to excite the self-oscillation and the microwave signal was generated via the GMR or AMR resistance oscillations and measured by a spectrum analyzer. Fig. 4.5(a) is the power spectral density amplitude of GMR-based SHO as functions of emission frequency and applied dc bias. An 800 G external field was applied in-plane perpendicular to the nanowire axis. (Hard axis) Fig. 4.5(c) shows the single spectra at 6 mA cross section line of Fig. 4.5(a). In comparison with the GMR-based SHO, Fig. 4.5(b) and (d) also shows the spectrum of AMR-based SHO and the cross section spectra at 3.65 mA. In order to

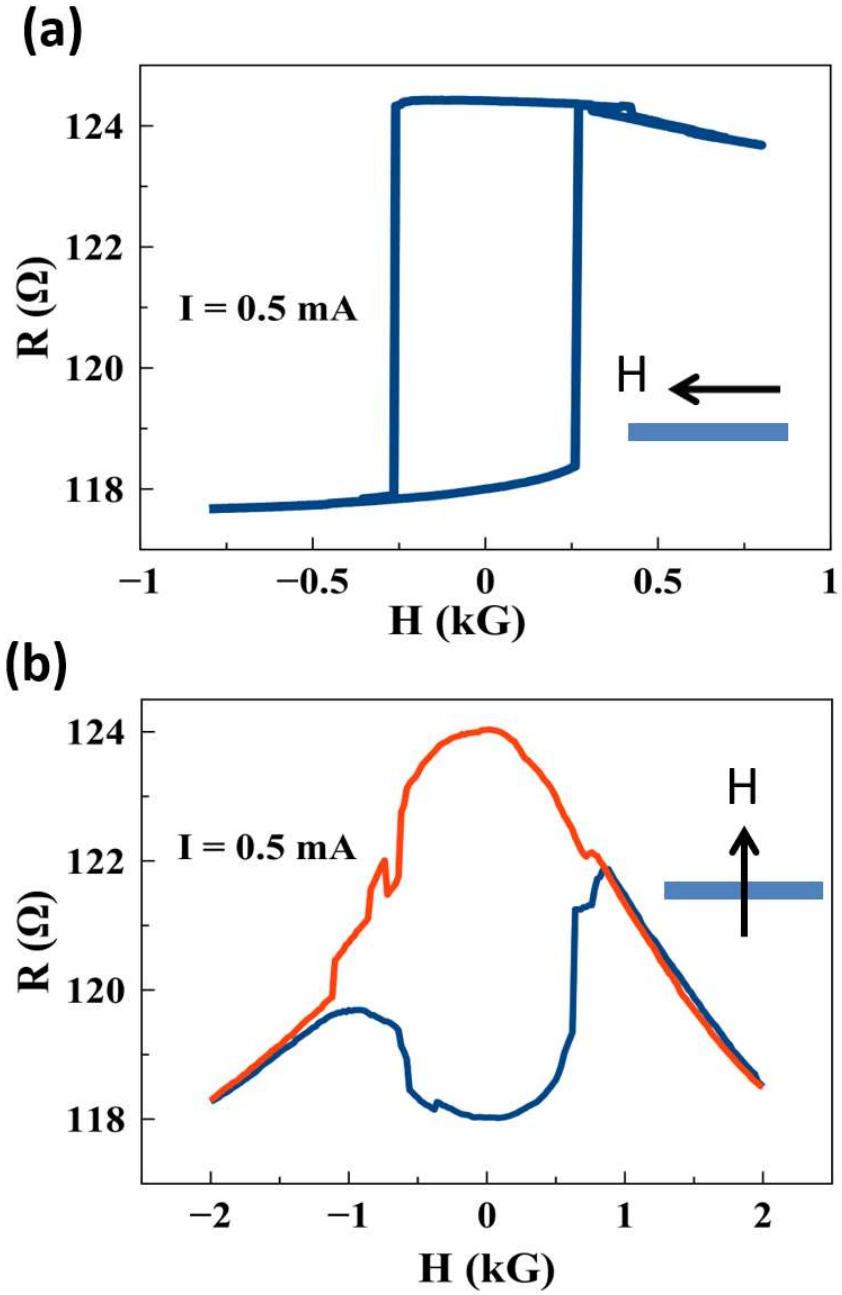

Figure 4.3: **(a)/(b)** The MR of the GMR-based SHO device with the magnetic field applying in-plane parallel to the easy/hard axis.

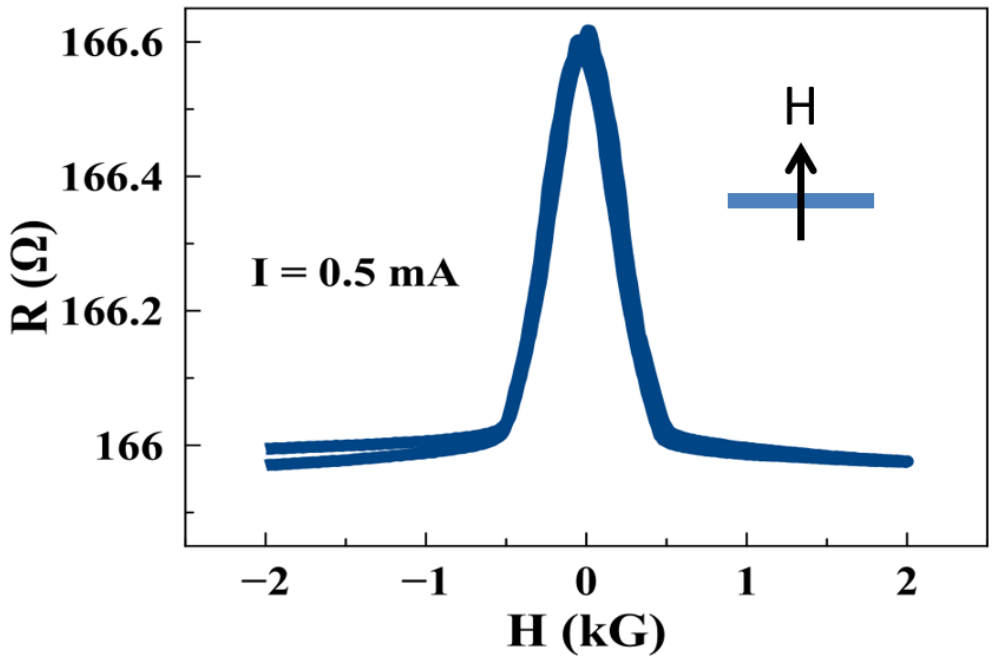

Figure 4.4: The MR of the AMR-based SHO device with the magnetic field applying in-plane parallel to the nanowire axis.

compare to the GMR-based SHO device with similar conditions, an 800 G external field was applied to the AMR-based SHO device 85 degree with respect to the nanowire axis (near perpendicular to the nanowire axis). In Fig. 4.5(a), the oscillation frequency increases as applied dc bias increases. This blue-shift behavior is likely from the dynamic dipolar interaction to the pinned cobalt layer oscillation modes. In previous reports [16, 20, 22], the frequency red-shifts of spectrum is usually observed in Pt/Py AMR-based SHO systems. One of the possible reasons is due to the dc bias induced oersted field exerting on the FM layer and decreasing the effective magnetic field. In the AMR-based SHO device which we reported in this letter, a copper layer was specifically added under the Permalloy (Py) layer. Since the current density flow through the top Pt layer is similar to the bottom Cu layer, there is no obviously shifting of spectrum (Fig. 4.5(c)) as a function of applied dc bias. To be noticed, the excitation bias current of GMR-based SHO is larger than the one of AMR-based SHO. Also, the linewidth of the self-oscillation mode of GMR-based SHO is larger than the

one of AMR-based SHO. (Fig. 4.5(c) and Fig. 4.5(d)) This implies that the thermal noise, which comes from the shunted current through the spin valve multilayer, on GMR-based SHO is greatly limiting the emission efficiency.

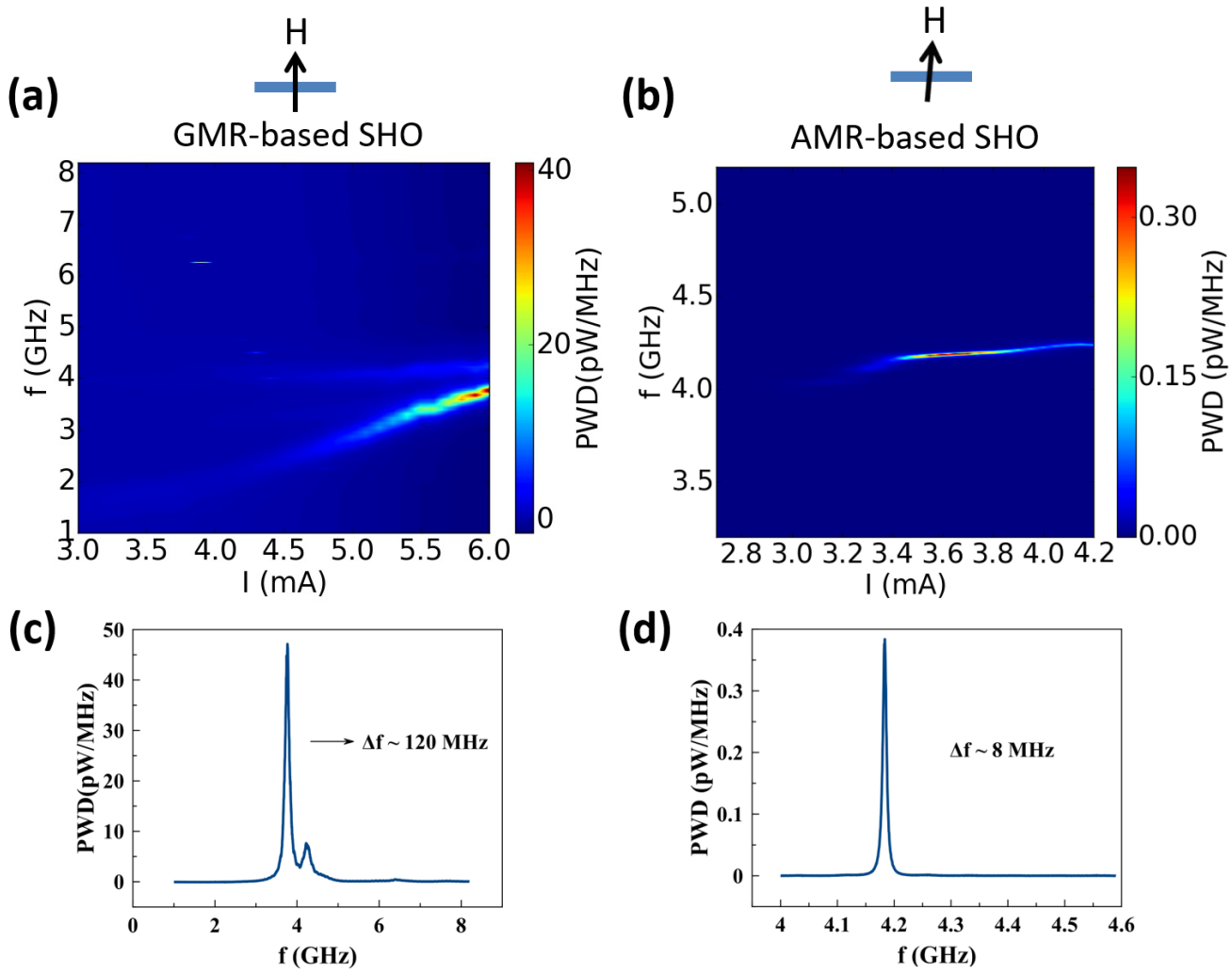

Figure 4.5: **(a)** Current bias (I_{dc}) dependent power spectral density (PSD) of GMR-based SHO device at $H = 800$ G. **(b)** Current bias (I_{dc}) dependent PSD of AMR-based SHO device at $H = 800$ G. **(c)** The PSD cross line profile of GMR-based SHO spectrum at $I_{dc} = 6$ mA. **(d)** The PSD cross line profile of AMR-based SHO spectrum at $I_{dc} = 3.65$ mA.

4.3 Integrated power analysis

Next we extracted out the integral microwave emission power of both devices for comparison. Figure 4.6 shows the integrated power as a function of applied dc bias current of both GMR-based SHO (blue curve) and AMR-based SHO (red curve). The Fig. 4.6(b) is the enlargement of the red curve in Fig. 4.6(a). The highest output power of the GMR-based SHO device happened at 6 mA is around 1.2 nW whereas the highest power of AMR-based SHO device is 4.6 pW at 3.6 mA. In an approximated evaluation, the microwave emission power is proportional to the square of current and GMR and AMR resistance differences. $P_{GMR(AMR)} \sim (I_{dc}\Delta R_{GMR(AMR)})^2$ By calculating the ratio from the equation, $P_{AMR}/P_{GMR} \approx 0.004$, this value is surprisingly matched to the experimental result. In our experiments, the integrated power of the GMR-based SHO did not reach the highest power output in Fig. 4.6(a), because we limited the applied bias current to protect of nano-geometry device. Therefore, the non-maxima power output usually demonstrates that the spin wave mode of GMR-based SHO is less coherent in oscillations and thus less emission power output than expected. However, the AMR-based SHO has been shown that maxima emission power should be happened while its magnetization equilibrium orientation is at 45 degree with respect to the nanowire axis. So the integrated power of AMR-based SHO taken at 85 degree with respect to nanowire axis (shown in Fig. 4.6(b)) is smaller in magnitude than that in the maxima position. Since both the GMR and AMR-based SHOs output less microwave power in our experimental configuration, this leads to the result to be quite reasonable.

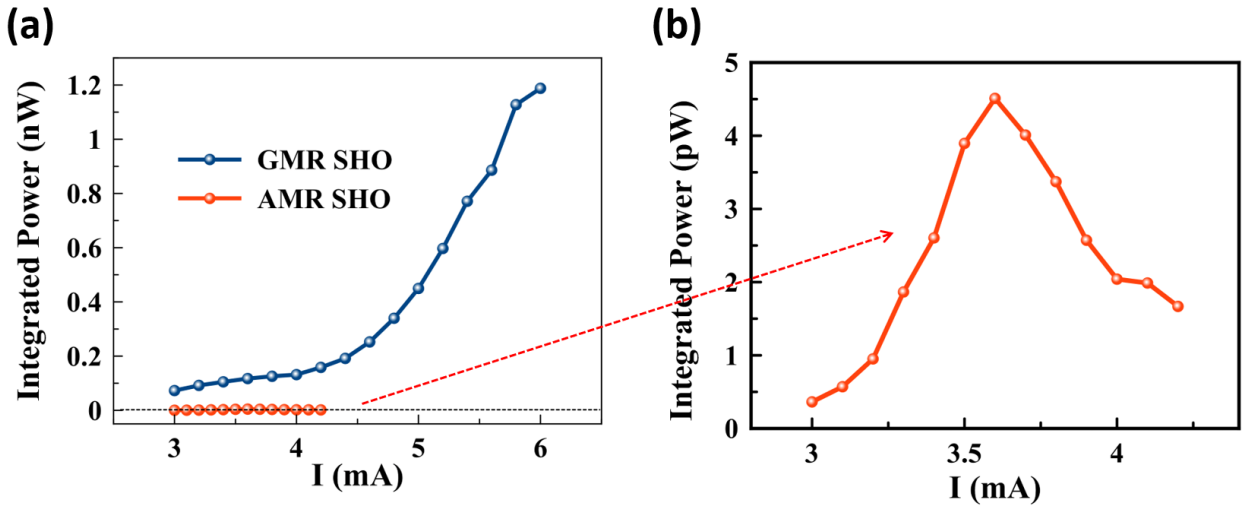

Figure 4.6: **(a)** The bias dependent auto-oscillation integral microwave power of GMR based SHO (blue) and AMR-based SHO (red). **(b)** The enlarge image of the red curve plotted in (a).

4.4 Angular dependence

As we mentioned in previous paragraphs, the output power of SHO is related to the oscillations of MR of FM layer, which depends on the magnetization orientation relative to a reference direction. This reference direction is the pinned FM layer direction of the GMR-based SHO, and its also the current flow direction of both GMR and AMR-based SHOs. In this report, we have it always along the nanowire direction. Therefore, the integrated power of SHOs possesses an angular dependence due to the origins of angular differences of AMR and GMR. The resistance oscillations can be written as the changes of the relative angles. $\delta R_{ac}\ \frac{\partial \Delta R(\theta)}{\partial \theta}\delta\theta(\omega,t)$. For GMR-based SHO, $\frac{\partial \Delta R_{GMR}}{\partial \theta} \sim sin(\theta)$, the maxima of resistance oscillation is happened at 90 degree with respect to nanowire axis. Whereas for AMR-based SHO, $\frac{\partial \Delta R_{AMR}}{\partial \theta} \sim sin(2\theta)$, the maxima is at 45 degree. Fig. 4.7 shows the integrated power angular dependence of both the GMR and AMR-based SHOs. A 500 G external field was applied at the angle θ related to the nanowire axis. The microwave emission signals were taken in a 90 degree range at a constant bias current. There is one single maximum of GMR-

based SHO at $\theta = 90$ degree and two maxims of AMR-based SHO at 70 and 110 degrees. Fig. 4.7(a) proves that the maxima power of GMR-based SHO is exactly at 90 degree angle and the power drops quickly when the external field is applied off from the 90 degree angle. In Fig. 4.7(b), the highest power output of AMR-based SHO is not at 45 degree instead it is symmetric and 20 degree off from the 90 degree angle. Since the demagnetization field of 1-D nanowire is much larger along the wire axis, the magnetization orientation is dragged toward the nanowire axis. Also, the spin orbit torque which comes from the spin Hall Effect in Pt layer is most efficiently transferred as an anti-damping torque at 90 degree. The threshold current of SHO possesses a trend as function of external field direction relative to the nanowire axis. So power maxima angles of AMR-based SHO should be in between the 45 and 90 degree angles as what we expected.

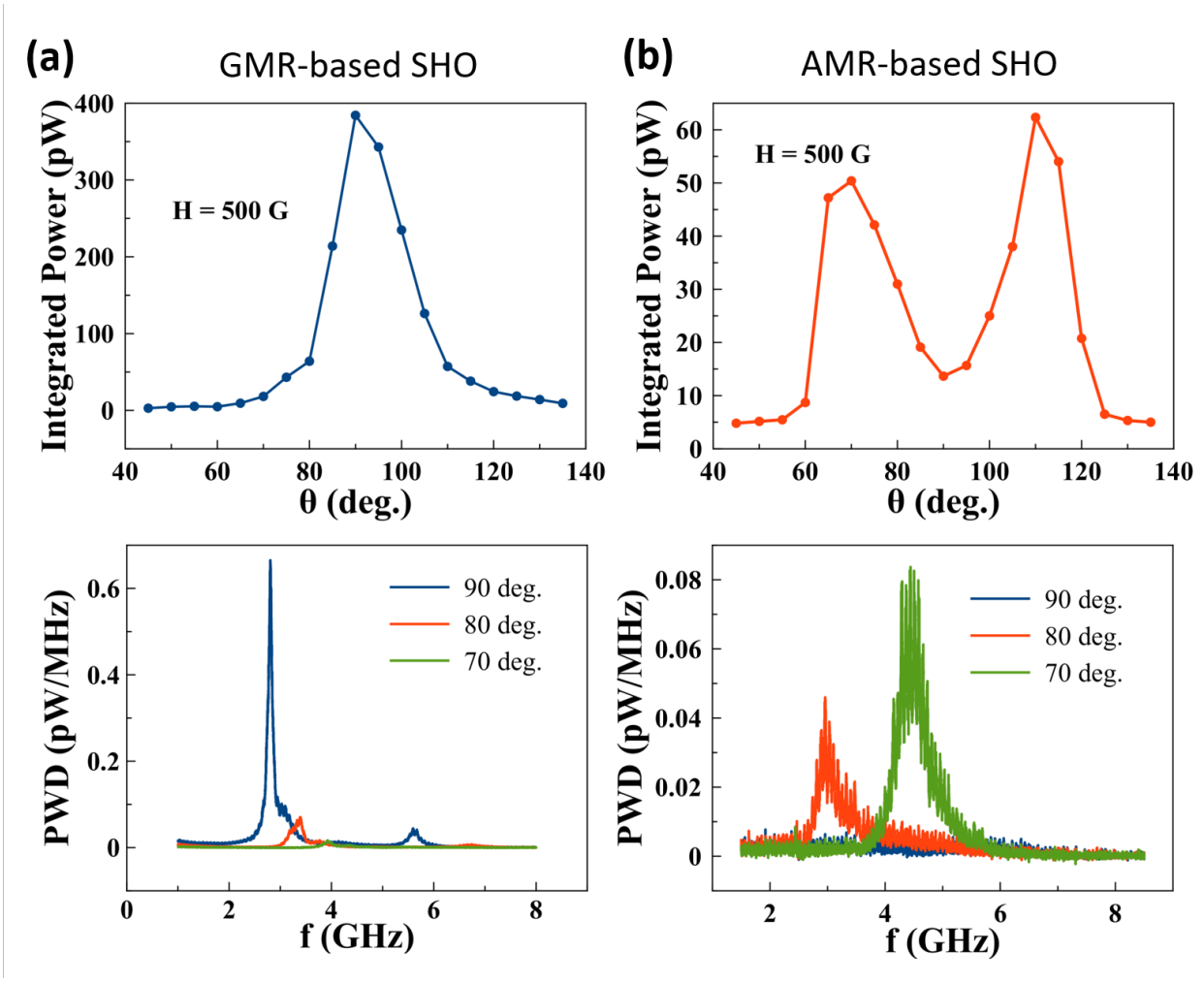

Figure 4.7: **(a)** The angular dependence of the integral power of GMR-based SHO at $H = 500$ G. θ indicates the angle of applied external field related to the nanowire axis. The bottom graph shows the single spectra of θ equals to 90, 80, and 70 degree. The integrated power decreases as the θ increases. **(b)** The angular dependence of the integral power of AMR-based SHO at $H = 500$ G.

Chapter 5

Conclusion

There have been lots of studies on different SHO systems, for example, nanogap contacts on heavy metal (HM)-FM disk, nano-constriction of Pt-Py bilayer structure, and 1D Pt-Py nanowire. In these SHO systems, the advantages include easier fabrication steps and direct optical measurement on the oscillation active region. However, these SHOs usually exhibit lower emission power output. By integrating the GMR stack into the SHO nanowire, we still keep the benefits of the SHO systems and also largely enhanced the output powers. The possible improvements of GMR-based SHO could be introduced and enhance the output powers even more. For example, the thermal stability can be increased by decreasing the distance of contact leads. The GMR stack could be optimized by increasing the stiffness of pinned layer and GMR ratio of devices. Recent study on multiple nano-constricted bilayer SHO devices have shown that the mutual synchronization of SHOs was achieved and enhanced the output power. The method which synchronizes multiple nano devices has been applied to both STO and SHO to increase output powers. This also promises the GMR-based SHOs to be able to reach sufficient power for real applications. We have shown that by integrating the GMR metallic spin valve stack into the SHO nanowire device, the output powers can be significantly enhanced. Remarkably, comparing to the conventional bilayer AMR-based SHO

system, the output powers can be increased more than an order of magnitude. Further, the simple fabrication of oscillators could be beneficial for developing and building into future electronic applications.

Bibliography

[1] Daniel C Ralph and Mark D Stiles. Spin transfer torques. *Journal of Magnetism and Magnetic Materials*, 320(7):1190–1216, 2008.

[2] M. N. Baibich, J. M. Broto, A. Fert, F. Nguyen Van Dau, F. Petroff, P. Etienne, G. Creuzet, A. Friederich, and J. Chazelas. Giant magnetoresistance of (001)fe/(001)cr magnetic superlattices. *Phys. Rev. Lett.*, 61:2472–2475, Nov 1988. doi: 10.1103/PhysRevLett.61.2472. URL `https://link.aps.org/doi/10.1103/PhysRevLett.61.2472`.

[3] G. Binasch, P. Grünberg, F. Saurenbach, and W. Zinn. Enhanced magnetoresistance in layered magnetic structures with antiferromagnetic interlayer exchange. *Phys. Rev. B*, 39:4828–4830, Mar 1989. doi: 10.1103/PhysRevB.39.4828. URL `https://link.aps.org/doi/10.1103/PhysRevB.39.4828`.

[4] Nevill Francis Mott. The electrical conductivity of transition metals. *In Proceedings of the Royal Society of London A: Mathematical, Physical and Engineering Sciences*, 153 (880):699–717, Feb 1936.

[5] J. E. Hirsch. Spin hall effect. *Phys. Rev. Lett.*, 83:1834–1837, Aug 1999. doi: 10.1103/PhysRevLett.83.1834. URL `https://link.aps.org/doi/10.1103/PhysRevLett.83.1834`.

[6] Shufeng Zhang. Spin hall effect in the presence of spin diffusion. *Physical Review Letters*, 85(2):393–396, 7 2000. ISSN 0031-9007. doi: 10.1103/PhysRevLett.85.393.

[7] Axel Hoffmann. Spin hall effects in metals. *IEEE transactions on magnetics*, 49(10): 5172–5193, 2013.

[8] John C Slonczewski. Current-driven excitation of magnetic multilayers. *Journal of Magnetism and Magnetic Materials*, 159(1-2):L1–L7, 1996.

[9] LALE Landau and Evgeny Lifshitz. On the theory of the dispersion of magnetic permeability in ferromagnetic bodies. *Phys. Z. Sowjetunion*, 8(153):101–114, 1935.

[10] TL Gilbert. Armour research foundation project no. *A05*, 1956.

[11] S. I. Kiselev, J. C. Sankey, I. N. Krivorotov, N. C. Emley, R. J. Schoelkopf, R. A. Buhrman, and D. C. Ralph. Microwave oscillations of a nanomagnet driven by a spin-polarized current. *Nature*, 425:380–383, 2003.

[12] Tingsu Chen, Randy K Dumas, Anders Eklund, Pranaba K Muduli, Afshin Houshang, Ahmad A Awad, Philipp Dürrenfeld, B Gunnar Malm, Ana Rusu, and Johan Åkerman. Spin-torque and spin-hall nano-oscillators. *Proceedings of the IEEE*, 104(10):1919–1945, 2016.

[13] L Berger. Emission of spin waves by a magnetic multilayer traversed by a current. *Physical Review B*, 54(13):9353, 1996.

[14] Andrei Slavin and Vasil Tiberkevich. Nonlinear auto-oscillator theory of microwave generation by spin-polarized current. *IEEE Transactions on Magnetics*, 45(4):1875–1918, 2009.

[15] Q Mistral, Joo-Von Kim, T Devolder, P Crozat, C Chappert, JA Katine, MJ Carey, and K Ito. Current-driven microwave oscillations in current perpendicular-to-plane spin-valve nanopillars. *Applied physics letters*, 88(19):192507, 2006.

[16] PM Braganca, BA Gurney, BA Wilson, JA Katine, S Maat, and JR Childress. Nanoscale magnetic field detection using a spin torque oscillator. *Nanotechnology*, 21(23):235202, 2010.

[17] William H Rippard, Matthew R Pufall, S Kaka, Stephen E Russek, and Thomas J Silva. Direct-current induced dynamics in co_90fe_10/ni_80fe_20 point contacts. *Physical Review Letters*, 92(2):027201, 2004.

[18] K Ando, S Takahashi, K Harii, K Sasage, J Ieda, S Maekawa, and E Saitoh. Electric manipulation of spin relaxation using the spin hall effect. *Physical review letters*, 101 (3):036601, 2008.

[19] Xin Fan, Jun Wu, Yunpeng Chen, Matthew J Jerry, Huaiwu Zhang, and John Q Xiao. Observation of the nonlocal spin-orbital effective field. *Nature communications*, 4:1799–1799, 2013.

[20] Jairo Sinova, Dimitrie Culcer, Q Niu, NA Sinitsyn, T Jungwirth, and AH MacDonald. Universal intrinsic spin hall effect. *Physical Review Letters*, 92(12):126603, 2004.

[21] Luqiao Liu, Takahiro Moriyama, DC Ralph, and RA Buhrman. Spin-torque ferromagnetic resonance induced by the spin hall effect. *Physical review letters*, 106(3):036601, 2011.

[22] Vladislav E Demidov, Sergei Urazhdin, Henning Ulrichs, Vasyl Tiberkevich, Andrei Slavin, Dietmar Baither, Guido Schmitz, and Sergej O Demokritov. Magnetic nano-oscillator driven by pure spin current. *Nature materials*, 11(12):1028–1031, 2012.

[23] RH Liu, WL Lim, and S Urazhdin. Spectral characteristics of the microwave emission by the spin hall nano-oscillator. *Physical review letters*, 110(14):147601, 2013.

[24] M Ranjbar, P Drrenfeld, M Haidar, E Iacocca, M Balinskiy, TQ Le, M Fazlali, A Houshang, AA Awad, RK Dumas, et al. Cofeb-based spin hall nano-oscillators. *IEEE Magnetics Letters*, 5:1–4, 2014.

[25] RH Liu, WengLee Lim, Sergei Urazhdin, et al. Dynamical skyrmion state in a spin current nano-oscillator with perpendicular magnetic anisotropy. *Physical review letters*, 114(13):137201, 2015.

[26] VE Demidov, S Urazhdin, A Zholud, AV Sadovnikov, and SO Demokritov. Nanoconstriction-based spin-hall nano-oscillator. *Applied Physics Letters*, 105(17): 172410, 2014.

[27] AA Awad, P Dürrenfeld, A Houshang, M Dvornik, E Iacocca, RK Dumas, and Johan Åkerman. Long-range mutual synchronization of spin hall nano-oscillators. *Nature Physics*, page 14, 2016.

[28] Zheng Duan, Andrew Smith, Liu Yang, Brian Youngblood, Jürgen Lindner, Vladislav E Demidov, Sergej O Demokritov, and Ilya N Krivorotov. Nanowire spin torque oscillator driven by spin orbit torques. *Nature communications*, 5:5616, 2014.

[29] Martin Collet, Xavier De Milly, O dAllivy Kelly, Vladimir V Naletov, Rozenn Bernard, Paolo Bortolotti, J Ben Youssef, VE Demidov, SO Demokritov, JL Prieto, et al. Generation of coherent spin-wave modes in yttrium iron garnet microdiscs by spin-orbit torque. *Nature communications*, 7:10377, 2016.

[30] Alexey V Nazarov, Konstantin Nikolaev, Zheng Gao, Haeseok Cho, and Dion Song. Microwave generation in mgo magnetic tunnel junctions due to spin transfer effects. *Journal of Applied Physics*, 103(7):07A503, 2008.

[31] Thibaut Devolder, Laurence Bianchini, Joo-Von Kim, Paul Crozat, Claude Chappert, Sven Cornelissen, Maaike Op de Beeck, and Liesbet Lagae. Auto-oscillation and narrow spectral lines in spin-torque oscillators based on mgo magnetic tunnel junctions. *Journal of applied physics*, 106(10):103921, 2009.

[32] Sumito Tsunegi, Kay Yakushiji, Akio Fukushima, Shinji Yuasa, and Hitoshi Kubota. Microwave emission power exceeding 10 μ w in spin torque vortex oscillator. *Applied Physics Letters*, 109(25):252402, 2016.

[33] Hitoshi Kubota, Kay Yakushiji, Akio Fukushima, Shingo Tamaru, Makoto Konoto, Takayuki Nozaki, Shota Ishibashi, Takeshi Saruya, Shinji Yuasa, Tomohiro Taniguchi, et al. Spin-torque oscillator based on magnetic tunnel junction with a perpendicularly magnetized free layer and in-plane magnetized polarizer. *Applied Physics Express*, 6 (10):103003, 2013.

[34] Zhongming Zeng, Pedram Khalili Amiri, Ilya N Krivorotov, Hui Zhao, Giovanni Finocchio, Jian-Ping Wang, Jordan A Katine, Yiming Huai, Juergen Langer, Kosmas Galatsis, et al. High-power coherent microwave emission from magnetic tunnel junction nano-oscillators with perpendicular anisotropy. *Acs Nano*, 6(7):6115–6121, 2012.

[35] IN Krivorotov, DV Berkov, NL Gorn, NC Emley, JC Sankey, DC Ralph, and RA Buhrman. Large-amplitude coherent spin waves excited by spin-polarized current in nanoscale spin valves. *Physical Review B*, 76(2):024418, 2007.

[36] PM Braganca, BA Gurney, AGF Garcia, JA Katine, and JR Childress. Dependence of nonlinearity and spectral linewidth on bias current in large-angle spin-torque oscillators. *Physical Review Applied*, 4(1):014017, 2015.

[37] Shehzaad Kaka, Matthew R. Pufall, William H. Rippard, Thomas J. Silva, Stephen E. Russek, and Jordan A. Katine. Mutual phase-locking of microwave spin torque nano-oscillators. *Nature*, 437:389–392, 2005.

[38] Ye Pogoryelov, PK Muduli, Stefano Bonetti, Fred Mancoff, and Johan Åkerman. Spin-torque oscillator linewidth narrowing under current modulation. *Applied Physics Letters*, 98(19):192506, 2011.

[39] Joo-Von Kim, Vasil Tiberkevich, and Andrei N Slavin. Generation linewidth of an auto-oscillator with a nonlinear frequency shift: Spin-torque nano-oscillator. *Physical review letters*, 100(1):017207, 2008.

[40] SSP Parkin. Origin of enhanced magnetoresistance of magnetic multilayers: Spin-dependent scattering from magnetic interface states. *Physical review letters*, 71(10): 1641, 1993.

[41] PA Grünberg. Exchange anisotropy, interlayer exchange coupling and gmr in research and application. *Sensors and Actuators A: Physical*, 91(1):153–160, 2001.

[42] Mannan Ali, Christopher H Marrows, M Al-Jawad, Bryan J Hickey, Arkajyoti Misra, Ulrich Nowak, and Klaus-Dieter Usadel. Antiferromagnetic layer thickness dependence of the irmn/co exchange-bias system. *Physical review B*, 68(21):214420, 2003.